ACSNANO
www.acsnano.org
ARTICLE

Sequential Infiltration Synthesis for the Design of Low Refractive Index Surface Coatings with Controllable Thickness

Diana Berman,[*,§,†] Supratik Guha,[‡,∥] Byeongdu Lee,[⊥] Jeffrey W. Elam,[†] Seth B. Darling,[‡,∥] and Elena V. Shevchenko[*,‡]

[‡]Center for Nanoscale Materials, [†]Energy Systems Division, and [⊥]Advanced Photon Source, Argonne National Laboratory, Argonne, Illinois 60439 United States

[§]Materials Science and Engineering Department, University of North Texas, Denton, Texas 76203 United States

[∥]Institute for Molecular Engineering, University of Chicago, Chicago, Illinois 60637 United States

Supporting Information

ABSTRACT: **Control over refractive index and thickness of surface coatings is central to the design of low refraction films used in applications ranging from optical computing to antireflective coatings. Here, we introduce gas-phase sequential infiltration synthesis (SIS) as a robust, powerful, and efficient approach to deposit conformal coatings with very low refractive indices. We demonstrate that the refractive indices of inorganic coatings can be efficiently tuned by the number of cycles used in the SIS process, composition, and selective swelling of the of the polymer template. We show that the refractive index of Al_2O_3 can be lowered from 1.76 down to 1.1 using this method. The thickness of the Al_2O_3 coating can be efficiently controlled by the swelling of the block copolymer template in ethanol at elevated temperature, thereby enabling deposition of both single-layer and graded-index broadband antireflective coatings. Using this technique, Fresnel reflections of glass can be reduced to as low as 0.1% under normal illumination over a broad spectral range.**

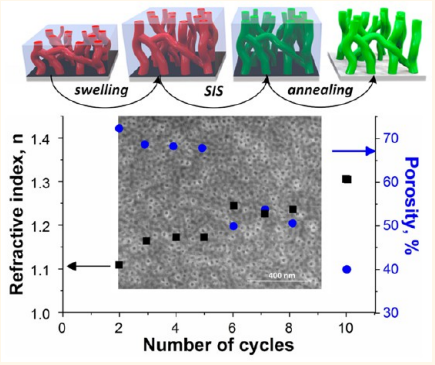

KEYWORDS: *antireflective, sequential infiltration synthesis, block copolymer, porous, low refractive index, polymer swelling*

A broad array of applications ranging from high-performance computing to antireflective coatings can benefit from the ability to manipulate refractive index in thin films. The refractive index of surface coatings is determined by a combination of composition and structure. The availability of materials with suitable refractive indices, especially for optical applications, is limited. Coatings with low refractive indices improve the performance of light emitting diodes, solar cells, and eye glasses.[1] Materials with refractive indices below 1.20 are highly desired for distributed Bragg reflectors used in waveguides and other high-performance optics; however, dense materials with such low refractive indices do not exist. The reduction of light reflected off surfaces relies on adjusting both the thickness and refractive index of the antireflective coating (ARC) in a way that the light reflected off two interfaces, such as air/coating and coating/substrate, interferes destructively. According to the Fresnel equation, this condition can be achieved for a given wavelength λ and angle of incidence when the thickness of the ARC is $\sim\lambda/4$ and refractive index of the ARC equals the square-root of the substrate refractive index. The ability to lower the refractive index of the materials is critical for the design of ARCs that help to minimize the reflection of the light and improve efficiency. For example, an ARC of MgF_2 on the surface of float glass can decrease the amount of the reflected light from 4.3% to almost 1% at the specified center wavelength and normal incidence, thereby increasing transmission in a given spectral range.[2]

ARCs on the surfaces of materials with relatively low refractive indices, such as fused glass (1.458), crown glass (1.485), sapphire glass (1.768), Gorilla glass (1.5), and polycarbonate (1.586) are of particular interest for corrective lenses, telescopes, and flat-panel displays. In telescopes that typically have several optical components, additive energy loss of reflected light can be substantial, hence effective ARCs are required. ARCs on flat-panel displays of electronic devices help eliminate stray reflections that cause unwanted veil glares. Single-layer MgF_2 (with a refractive index of 1.38) is the most commonly used ARC for surfaces with low refractive index. Even though its performance is not exceptional, it still provides

Received: December 13, 2016
Accepted: January 31, 2017
Published: January 31, 2017

DOI: 10.1021/acsnano.6b08361
ACS Nano 2017, 11, 2521−2530

decent antireflective properties in the middle of the visible band and works reasonably well for the entire spectral range.[3] Better performing ARCs for surfaces with low refractive indices typically consist of several metal oxide layers (*e.g.*, TiO_2, ITO, *etc.*), SiO_2, and polymers.[4] While one's ability to prepare high refractive index coatings is limited by the nature of available materials, the refractive index of optical films can be lowered by inducing suboptical porosity. For example, the refractive index of bulk silica (SiO_2) is 1.46; however, nanoporous SiO_2 films with refractive index of 1.08 have been reported,[5] which represents a value far below the lowest refractive index known for dense inorganic materials, such as 1.38 for MgF_2.[6] Widely used conventional single-layer ARCs target only a particular wavelength at normal incidence, while graded-index coatings allow omnidirectional broadband properties.[7] ARCs can be deposited (i) chemically, for example, by spin-casting of silica sols[8] or by layer-by-layer (LBL) deposition of charged colloids and polymers,[9,10] (ii) using vacuum-based coating techniques,[7] or (iii) by texturing the surface using lithographic and chemical approaches (*e.g.*, *via* etching).[11−15] These methods allow synthesis of porous films with different degrees of control over the film porosity. Since polymers are typically less stable against heat and UV light compared to inorganic materials,[16] porous inorganic coatings are preferred for a broad range of applications. When employing chemical approaches, the porosity of inorganic films can be tuned mainly by the size of the particles in the deposited nanoparticle arrays or by the size of the introduced polymeric fillers that are subsequently removed by solvent treatment or oxidative annealing.[17] Chemical approaches are straightforward for single-layer ARCs; however, they do not work well for graded-index coatings. Also, chemical deposition efforts have largely focused on silica coatings, which limits the control over the refractive index. Physical vapor deposition performed at a glancing angle yields nanostructured films with controllable porosity as a result of the self-shadowing effect and surface diffusion.[18] This technique has achieved the record low refractive index of 1.05.[7] In vacuum methods, graded-index ARCs are obtained *via* deposition of a number of layers with different porosity and composition. Such methods are usually applied for ARCs on small area surfaces due to their high cost of fabrication.

In general, the tuning of the refractive index of ARCs is a labor-intensive process, both in physical and chemical approaches. Lithographic and physical methods can produce ARCs with finely tuned refractive indices, resulting in excellent optical performance, however, this is achieved at the expense of high cost. In turn, the cost of chemically fabricated ARCs is reasonable; however, their performance is somewhat compromised, mainly because of the inability to finely control the refractive index. Design of multilayered ARCs by chemical methods, such as sol−gels, dipping or spinning processes, is challenging since each layer requires thermal annealing that can alter the porosity in the previously deposited layers affecting their optical properties. Also, chemical methods based on etching are not well suited to fabricate gradient structures due to potential impact of the etching agents on structures fabricated in the previous steps. However, the biggest challenge for ARCs on surfaces with low refractive indices is that regardless of the fabrication method, state-of-the art graded-index ARCs on surfaces with low refractive indices assume the initial deposition of coatings with high refractive indices. This step of artificial increase of refractive index of the surface is needed since there is only a limited number of materials (and approaches leading to materials) with refractive index <1.5.

Here we propose an efficient combined chemo-physical approach to finely control refractive index that can be used for single-layer and graded-index surface ARC coatings. The strategy is based on sequential infiltration synthesis (SIS), which involves diffusion-controlled penetration and subsequent chemisorption of inorganic precursor molecules inside a polymer template. In SIS, the precursors are introduced to the substrate in the vapor phase. Following SIS, the polymer matrix is removed *via* thermal annealing. When using block copolymer (BCP) films as substrates for SIS, one can achieve growth of the inorganic phase selectively within one of the polymer blocks. In this way, the self-assembled nanostructures of the BCP can be replicated in a functional, inorganic material. As SIS is diffusion controlled, growth within thick films can be cumbersome with difficult to predict reaction kinetics.[19] In this study, we report that swelling of the block copolymer template in ethanol at different temperatures prior to SIS efficiently tunes the thickness and porosity of the resulting ARCs and enables the fabrication of optical surface coatings for a desired spectral range. Solvent-assisted SIS can also produce multilayered graded index structures to deposit broadband ARCs. We believe the solvent-assisted SIS approach offers an opportunity to eliminate the commonly accepted artificial increase of surface refractive index in broadband multilayered ARCs for the materials with low refractive indices.

RESULTS AND DISCUSSION

When SIS is performed on a polymer such as poly(methyl methacrylate) (PMMA), the vapors of the inorganic precursor molecules infiltrate the bulk of the film and react with C═O and −C−O−R functional polar groups of the polymer macromolecule.[19−21] In the case of diblock copolymers with a purely hydrocarbon block, such as polystyrene (PS), connected to a block exhibiting polar groups (*e.g.*, PS-*b*-PMMA), the overall molecular weight and the volume fractions of the two blocks determine the morphology and size of the nanoscopic domains, which serve as a template for the SIS processed material. Earlier studies demonstrated that SIS in diblock copolymer films is a strategy to synthesize nanophase inorganic materials and to improve the quality of lithographically prepared features.[22,23] However, the optical properties of SIS-modified diblock copolymers have not yet been explored.

In this work, we demonstrate the ability to tune refractive indices by SIS and utilize this capability to synthesize antireflective coatings. We studied two types of block copolymers, polystyrene-*block*-poly(methyl methacrylate) (PS-*b*-PMMA) and poly(styrene-*block*-4-vinylpyridine) (PS-*b*-P4VP), as templates for SIS of inorganic materials with tunable refractive indices and antireflective properties.

PS-*b*-PMMA is one of the most popular BCPs and is frequently used in SIS.[20,24−26] PS-*b*-PMMA has been used as a template to pattern ZnO, Al_2O_3, SiO_2, TiO_2, W and other materials with different degrees of control over periodicity and structure.[19−21,27] Al_2O_3 SIS, in particular, has a robust chemistry with well-understood kinetics. Thus, we chose PS-*b*-PMMA-templated Al_2O_3 SIS as a model system for this study. Spin-casting 2 wt % toluene solutions of PS-*b*-PMMA with different percentage of PS followed by 1 h thermal annealing in argon atmosphere at 180 °C resulted in uniform, 70 ± 5 nm-thick films with microphase-separated domains. Since the long-

DOI: 10.1021/acsnano.6b08361
ACS Nano 2017, 11, 2521−2530

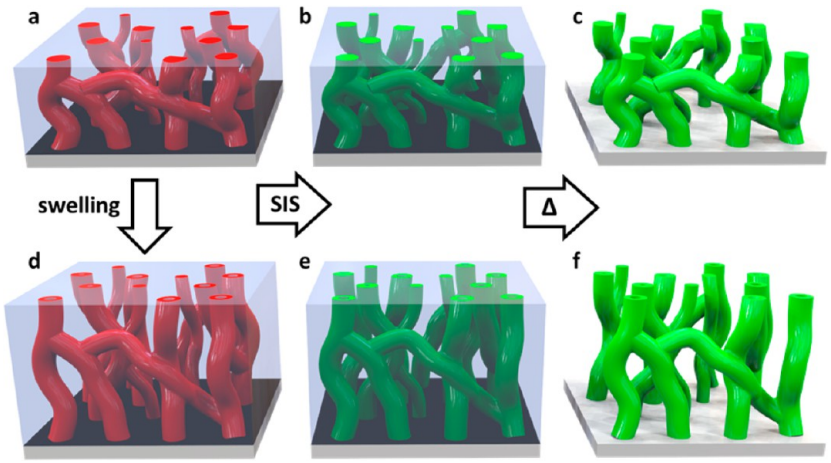

Figure 1. Depiction of the SIS (a–c) and solvent-assisted SIS (d–f) procedures leading to formation of porous Al_2O_3 coatings. Hydrophilic polymer domains (*e.g.*, PMMA or P4VP, shown in red) are infiltrated with the precursor of Al_2O_3 (shown in green) and converted into porous Al_2O_3 upon oxidative annealing.

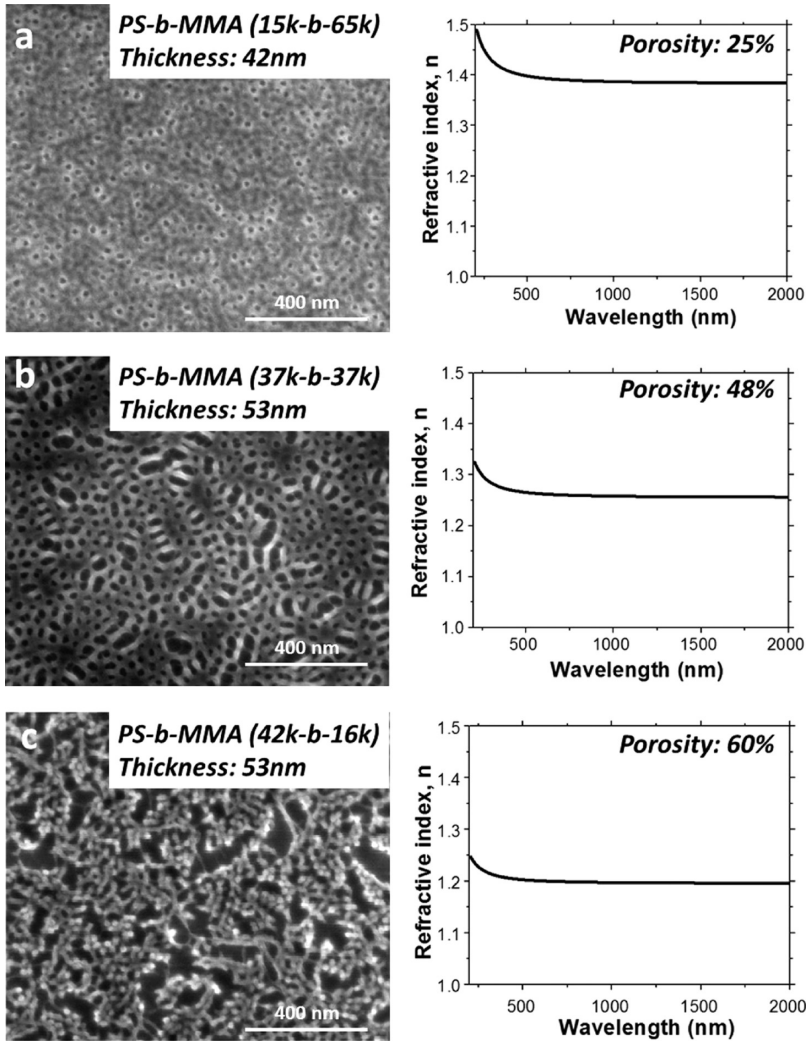

Figure 2. SEM images and the corresponding refractive indices of porous alumina films grown by the infiltration (5 SIS cycles) of PS-*b*-PMMA polymers with different volume fraction of polystyrene: (a) 15k-*b*-65k, (b) 37k-*b*-37k, and (c) 42k-*b*-16k.

range periodicity of structures at a scale far below the wavelength of visible light is not expected to affect the refractive index of the material, we did not perform additional procedures to induce long-range orientational order.[28,29]

Stepwise exposure of PS-*b*-PMMA to vapors of trimethylaluminum (TMA) and water during 5 cycles of SIS led to the growth of Al_2O_3 within the PMMA domains. Next, the polymer template was removed by oxidative thermal annealing for 1 h at

DOI: 10.1021/acsnano.6b08361
ACS Nano 2017, 11, 2521–2530

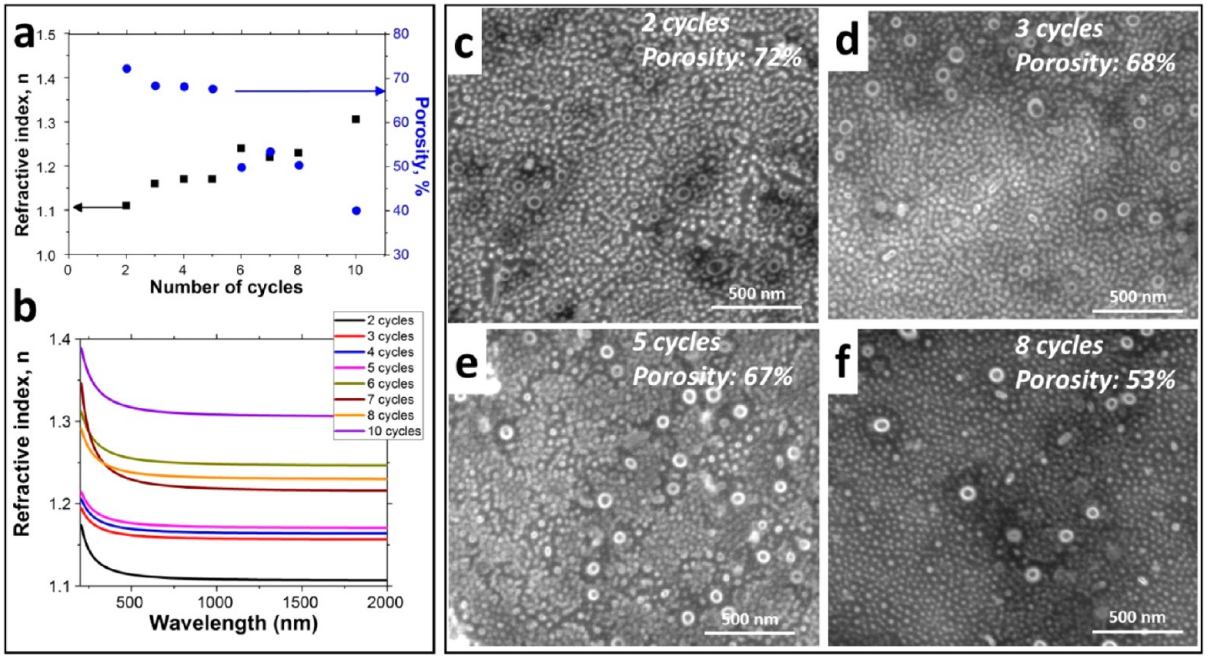

Figure 3. Porous alumina films grown by the infiltration of PS-*b*-P4VP with TMA/water as a function of number of SIS cycles. (a) Refractive indices measured at 785 nm wavelength and porosity show variation with the number of cycles. (b) Refractive index values *vs* wavelength for films obtained with different numbers of SIS cycles. (c) Representative SEM images of the grown Al_2O_3 films demonstrate evolution of the material structure as a function of the SIS cycle number. The thickness of the films shown in (c–f) is 48.7 ± 5.1 nm.

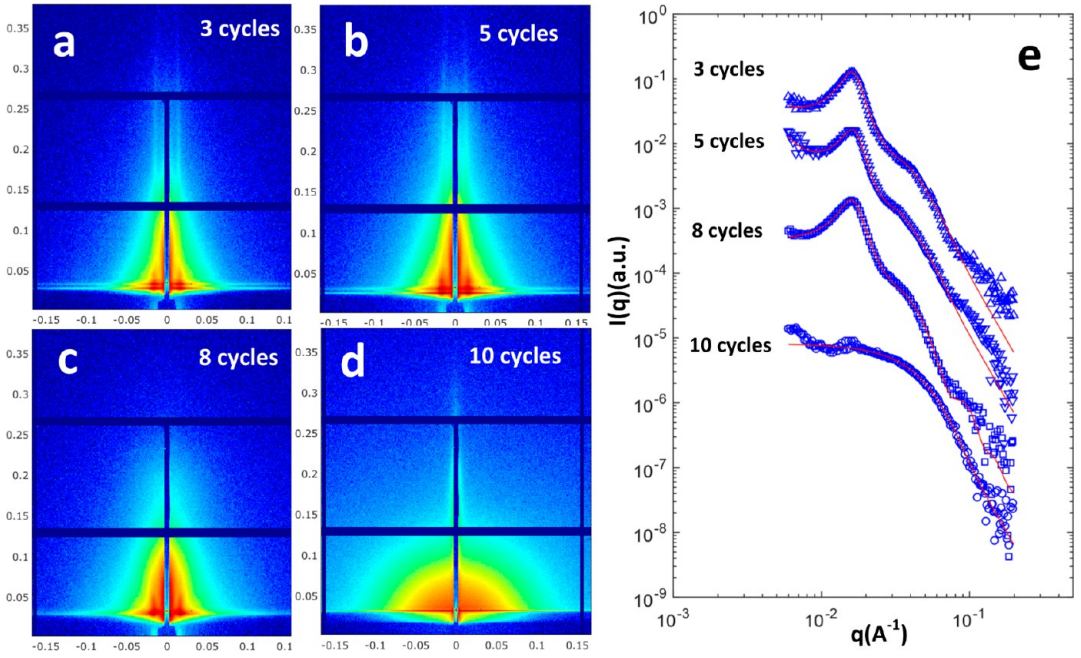

Figure 4. GISAXS (a–d) and transmission SAXS (e) data and fit (solid red line) for Al_2O_3 SIS films obtained with different number of SIS cycles. In (e), the data are arbitrarily scaled for better visualization.

450 °C. Figure 1 captures the processes involved in the formation of porous metal oxide films by infiltration of polymers without (a–c) and with swelling (d–f). The oxidative annealing of the SIS films proved to be more efficient than either ozone or plasma etching, which resulted in bubbling and rupture of the Al_2O_3 films due to rapid release of CO_2 (Figure S1).

Figure 2 shows SEM images of thin Al_2O_3 films with a different degree of porosity controlled by the PS/PMMA ratio on a silicon surface. Ellipsometry reveals that refractive indices are inversely proportional to the porosity and vary from 1.2 at 60% porosity to 1.39 at 25% porosity at a wavelength of 785 nm. These values are far below the 1.768 value characteristic to bulk alumina and also significantly below the value of 1.6 for amorphous ALD Al_2O_3.[30] Thus, we have demonstrated tuning of refractive indices of Al_2O_3 SIS films and satisfied one criterion for design of ARCs. The thickness of these films was not sufficient to provide antireflective properties to the coatings

DOI: 10.1021/acsnano.6b08361
ACS Nano 2017, 11, 2521–2530

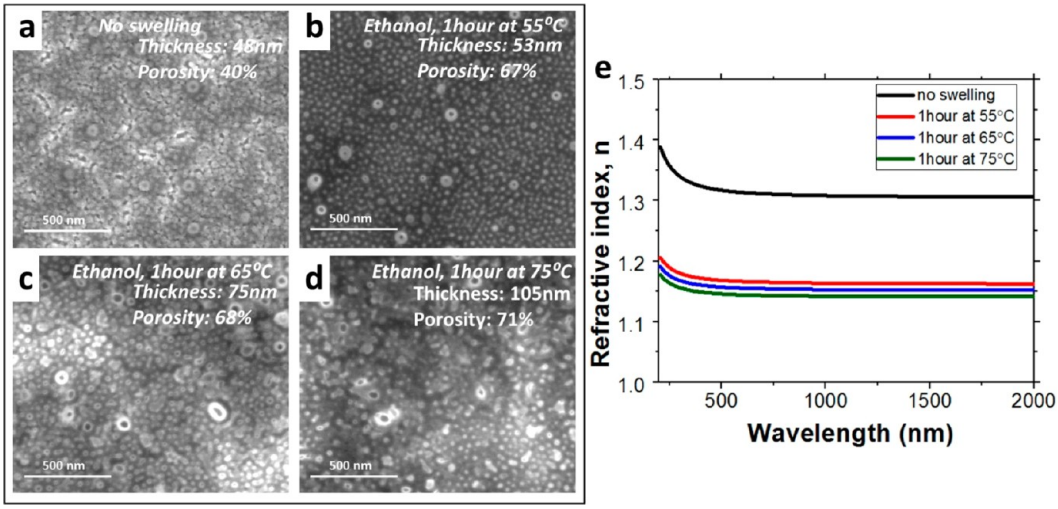

Figure 5. Porous alumina films grown by the infiltration of PS-*b*-P4VP polymers (10 cycles) without swelling in ethanol (a) and after swelling for 1 h at different temperatures at 55 °C (b), 65 °C (c), and 75 °C (d). The refractive indices of alumina films obtained with no polymer swelling and at different swelling regimes (e).

in the spectral range above 200 nm. Increase in the thickness of the PS-*b*-PMMA template achieved by increase of the concentration of the polymer in toluene solution did not lead to thicker final Al_2O_3 films, likely due to limited diffusion of TMA through the as-deposited film under these SIS conditions.

Swelling of BCPs in certain solvents was previously reported to induce porosity that potentially could assist the growth of thicker SIS films.[31] Swelling of our polymer templates with acetic acid, a procedure that worked well for periodic pre-aligned PS-*b*-PMMA,[31] was found to be partially successful. Acetic acid swelling allowed us to increase the overall thickness of the Al_2O_3 SIS films; however, the films were laterally non-uniform and were rather rough. In an effort to integrate swelling-induced porosity with a more controllable morphology, we turned our attention to another polymer system, PS-*b*-P4VP, as this is a model system for studying swelling phenomena in polymers.[32]

First, we conducted the set of experiments to confirm that PS-*b*-P4VP would work as an efficient template for deposition of alumina by SIS. We used a 2 wt % of PS-*b*-P4VP (75k-*b*-25k) BCP solution in toluene to spin-cast 80 nm-thick polymer templates and successfully obtained porous Al_2O_3 with refractive indices in the range between 1.11 and 1.25 following Al_2O_3 SIS and heat treatment procedures (Figure 3). We found that the porosity could be tuned by adjusting the number of SIS Al_2O_3 cycles. In particular, the porosity decreased monotonically with the number of SIS Al_2O_3 cycles. Dispersion of feature sizes in the Al_2O_3 SIS films prepared using PS-*b*-P4VP is a result of polydispersity present in the BCP material (most likely due to the presence of homopolymer) causing some size distribution of P4VP domains. The thickness of the alumina films produced by SIS, as measured by ellipsometry, was 48.7 ± 5.1 nm.

Grazing incidence small-angle X-ray scattering (GISAXS) patterns of samples prepared with 3 and 5 SIS cycles are similar (Figure 4). Both patterns presented a peak at q_y = 0.0165 Å^{-1}, indicating 2D nanostructures laterally ordered with a *d*-spacing of ~38 nm. GISAXS pattern obtained for the sample with 3 SIS cycles allowed for estimation of the thickness of the Al_2O_3 film as ~45 nm, which is in agreement with the ellipsometry data (Table S1). The shape of the peaks is generally a circular spot along the vertical direction, indicating that the lateral structure is as tall as the film thickness, although the peaks' weak vertical tails suggest coexistence of smaller features. The vertical sizes of the smaller features ranged from 5.0 to 6.0 nm and increased slightly with the number of SIS cycles. These values, obtained by fitting the data to a polydisperse sphere model, are summarized in Table S1. We also found at least two feature sizes along the horizontal direction, which are about 25 and 10 nm, respectively. These scattering results suggest that Al_2O_3 pillars seen in Figure 3 are made of smaller Al_2O_3 grains. After 10 SIS Al_2O_3 cycles, the sample completely lost lateral ordering peaks, and only randomly distributed spherical 8 nm particles are observed, indicating that the Al_2O_3 particles are probably grown on the surface of the polymer film. Electron densities obtained from the GISAXS patterns[33,34] are 0.243, 0.214, 0.403, and ~0.7 e/Å^3 for Al_2O_3 SIS films obtained with 3, 5, 8, and 10 SIS cycles, respectively. Considering the electron density of Al_2O_3 is 1.17 e/Å^3, their porosities of 2−5, 8, and 10 SIS cycles are 80, 65, and 40%, respectively. The summary of the GISAXS and SAXS data is given in Table S1. Ellipsometry measurements estimated the porosity of the same structures as 68, 58, and 40%, which is in relatively good agreement with SAXS data.

We have demonstrated that Al_2O_3 SIS in PS-*b*-P4VP templates yields even lower refractive indices values compared to PS-*b*-PMMA. However, as in the case of PS-*b*-PMMA, increasing the thickness of the PS-*b*-P4VP template did not increase the resulting Al_2O_3 film thickness beyond ~48 nm, which again relates to slow diffusion of the TMA precursor through the free volume of the PS-*b*-P4VP film. In order to introduce porosity to enhance diffusivity, we explored swelling. Swelling is a nondestructive strategy to induce and modify the porosity in BCP materials.[31] It is performed by immersing the BCP film in a solvent that is selective to the minority block. Upon drying, pores are generated throughout the film in the positions where the minority block has collapsed. Swelling of PS-*b*-P4VP in ethanol at different temperatures allows the formation of interconnected pores in the range between 10 and 50 nm.[31] These pores are much larger than the molecular-scale pores that define the polymer-free volume. Given that Knudsen diffusion scales as the diameter squared,[35] we expect a much more rapid and effective infiltration of the TMA into the

DOI: 10.1021/acsnano.6b08361
ACS Nano 2017, 11, 2521−2530

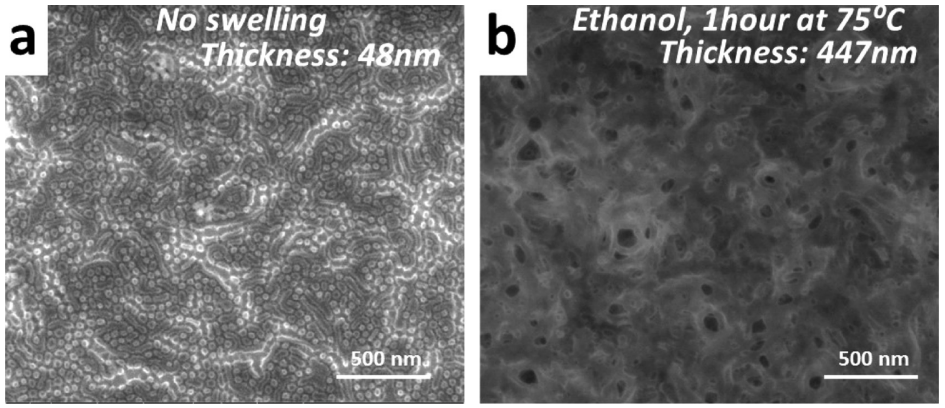

Figure 6. Porous alumina films grown by the infiltration during 5 SIS cycles of spin-cast 400 nm-thick PS-*b*-P4VP polymer (75k-*b*-25k) templated without swelling (a) and (b) after swelling at 75 °C for 1h.

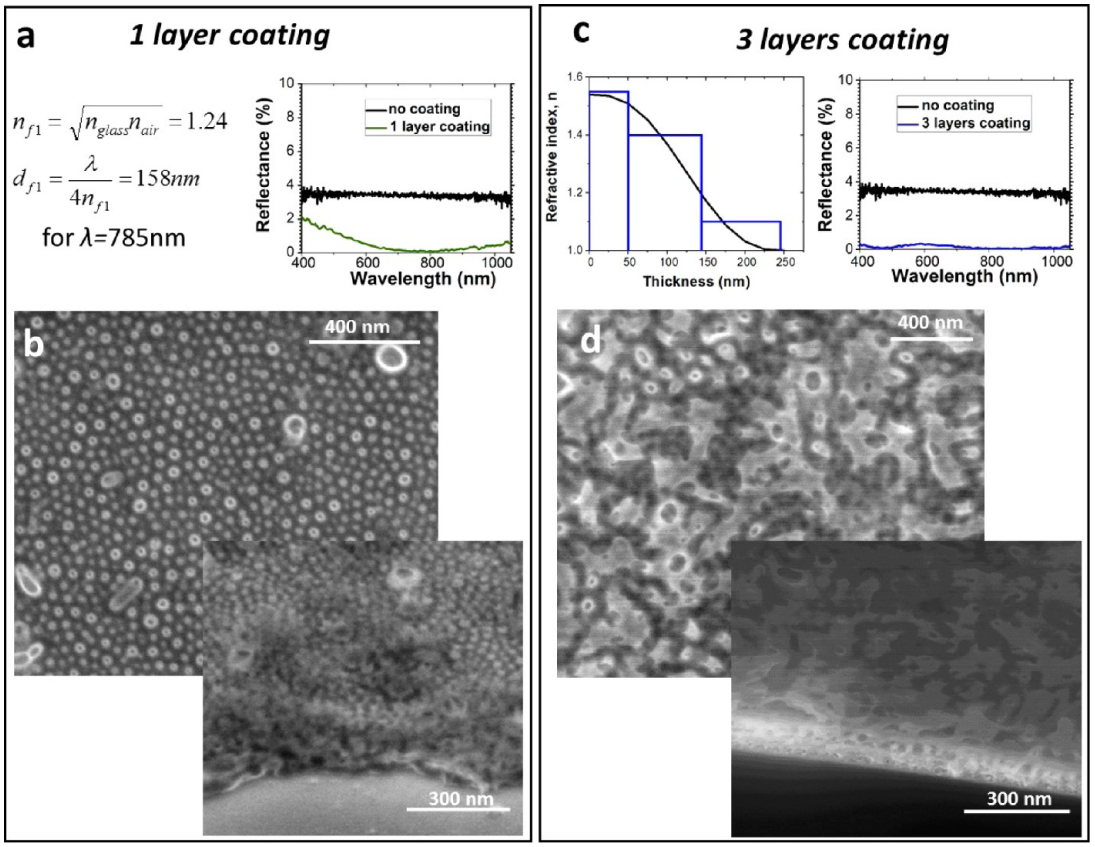

Figure 7. Two cases of antireflective coatings with single wavelength minimized reflection (a,b) and wide range minimized reflection deposited on the glass substrate (c,d). Figures (b) and (d) demonstrate the SEM images of porous Al_2O_3 coatings on silicon substrate fabricated by solvent-assisted SIS technique using the same synthesis parameters that were used for deposition on a glass substrate. Porous Al_2O_3 film deposited on glass with the use of PS-*b*-P4VP (75k-*b*-25k) precursor demonstrates minimized reflection for 785 nm light in comparison to bare glass (a); a three-layer Al_2O_3 deposited on glass in sequence with the assistance of three different polymer films demonstrates reduced reflection over the broad wavelength range of 400−1050 nm (c).

solvent-treated PS-*b*-P4VP films compared to the untreated films.

We immersed 80 nm-thick PS-*b*-P4VP films for 1 h in ethanol at different temperatures. After drying the samples under dry nitrogen for 10 min to remove excess ethanol, the Al_2O_3 SIS was performed. We increased the number of SIS cycles to 10 in order to target thicker films. Figure 5a demonstrates that Al_2O_3 SIS films prepared with 10 SIS cycles are still porous but rather dense. The porosity of the film estimated by ellipsometry is ∼40%, which is in a good agreement with SAXS data (Figure 4e). Figure 5b−d shows that swelling of the PS-*b*-4PVP template at different temperatures increases the porosity of the Al_2O_3 films, resulting in substantially lower refractive indices (Figure 5e). More importantly, the polymer swelling also yielded thicker Al_2O_3 SIS films. Figure 1 depicts the effect of swelling on the morphology of the final Al_2O_3 films. The Al_2O_3 films prepared using an untreated 80 nm-thick PS-*b*-P4VP template were only ∼48 nm in thickness. However, swelling the 80 nm-thick PS-*b*-P4VP template films in ethanol at temperatures of 55, 65, and

DOI: 10.1021/acsnano.6b08361
ACS Nano 2017, 11, 2521−2530

75 °C yielded Al_2O_3 film thicknesses of 53, 75, and 105 nm, respectively. We attribute this increase in thickness to the more effective diffusion of TMA through the 10−50 nm void spaces remaining after removing the PS component of the polymer template films.

The refractive indices of the Al_2O_3 SIS films obtained at different swelling temperatures were in the range between 1.17 and 1.14. These values are far below the lowest refractive index known for bulk inorganic materials such as the widely used MgF_2 in the design of ARCs.[36] The swelling property of the BCP is essential for the deposition of ARCs since it allows for tuning the thickness of the surface coating, which is critical for achieving a low reflectivity in a specific, targeted spectral range. Figure 6 shows that swelling of a 400 nm-thick PS-*b*-P4VP film in ethanol for 1 h at 75 °C leads to a 447 nm-thick porous Al_2O_3 SIS film, while no swelling results in the thickness limited by ∼48 nm value (Figure 6a).

With control established over both the refractive index and thickness of the deposited films, we proceeded to explore the SIS process to prepare ARC coatings. For a single-layer ARC, light reflection will be minimized when the coating satisfies certain criteria for its refractive index and thickness. The refractive index of the antireflection coating (n_{fl}) should be $n_{fl} = \sqrt{n_s n_{air}}$, where n_s and n_{air} are the refractive indices of the substrate and air, respectively. The optimum thickness of the ARC (d_{fl}) should be $d_{fl} = \frac{\lambda_0}{4n_1}$, where λ_0 is the wavelength of the light to be fully transmitted. For example, in order to eliminate the reflection of 785 nm wavelength light at a glass substrate with refractive index of 1.54, an 158 nm-thick ARC with refractive index of 1.24 is required. We prepared such an Al_2O_3 SIS coating by spin coating 80 nm-thick PS-*b*-P4VP and swelling it at 75 °C, followed by 10 SIS cycles. The thickness of this coating was 152 ± 8 nm, and the refractive index was 1.24. Reflectivity measurements indicate that only 0.1% of the light is reflected at ∼780 nm, while the uncoated glass substrate reflected ∼4% (Figure 7a). Figure 7a demonstrates that, in fact, the deposited single-layer Al_2O_3 SIS coating lowered the reflectivity in the entire 400−800 nm spectral range.

The main challenge for synthesis of ARCs that can eliminate the Fresnel reflection over a broad spectral range is unavailability of materials with very low refractive indices that can closely match the refractive index of air. Light reflection is minimized when the coating refractive index exhibits a continuous gradient change along the thickness from the value of the substrate material at the substrate/coating interface down to the air refractive index at the coating/air interface.[37−39] The deposition of films with uniform gradient change is challenging. Previous studies have demonstrated dramatic reduction in the light reflection for a coating made of several discrete layers with different constant refractive indices.[7] Control over the refractive index in graded-index structures of this nature minimized reflectivity over a broad spectral range.[7] Previous studies demonstrated that this goal can be achieved by deposition of layers of certain materials with controlled thickness and porosity by oblique-angle deposition. However, even though oblique-angle deposition obtained a record low refractive index of 1.05 for multilayers of TiO_2 and SiO_2, it is challenging to use this method for larger scales.

We explored the potential of SIS to design graded-index ARCs. To this end, we deposited three stacked layers of Al_2O_3 SIS films. Figure 7c shows the strategy we followed in terms of parameters selected for each layer. In order to minimize the reflectivity of the glass surface in spectral range 400−1050 nm, a minimum of three layers with the following refractive indices and thicknesses are required: 1.54 and 50 nm (first layer); 1.4 and 190 nm (second layer); and 1.1 and 200 nm (third layer). First layer was obtained by SIS using 80 nm-thick PS-*b*-PMMA and 10 SIS cycles. PS-*b*-P4VP templates of 80 nm and 10 and 5 SIS cycles, respectively, were used to form the second and third layers. The first and second layers were annealed at 450 °C under air flow for 1 h to remove the polymer prior to spin-casting of the second and third layers of a polymer template, correspondingly.

As evidenced from SEM imaging, the final film is porous and rather uniform (Figure 7d). Wavelength dependence of specular reflectivity demonstrated that the glass with three layers of Al_2O_3 SIS coating reflects between 0.4% and 0.1% of the light in the range of 400−1050 nm at normal incidence. Photographs of the uncoated glass and glass with single and multilayer coatings with optical characteristics are shown in Figure 8. The blue background in the area covered by uncoated glass is darker as compared with the uncovered area, whereas there is no visually detectable difference in the color of the blue background in the areas uncovered and covered with glass substrates with single- and three-layered ARCs. In order to quantify this observation, we analyzed the color of the images shown in Figure 8a in the areas uncovered (n) and covered with glass substrates (n*). We compared the color histograms in the areas covered by coated glass within the neighboring uncovered areas. Figure 8b demonstrates that the significant shift toward the darker color is observed in the area covered by plain glass, while a minor shift and no change in color histogram are observed for one- and three-layer coatings, respectively. These data indicate better light transmittance and the absence of residual carbon in the thermally annealed films. Energy dispersive X-ray analysis confirms that no carbon remains in the thermally annealed samples (Figure S2). As shown in Figure 8c, transmittance increased from ∼92.5% (uncoated glass sample) to ∼96.5% in a narrow range around 785 nm for the single-layer coated sample. In the case of three-layer films, the transmittance is improved to ∼95% in the whole visible light spectral range. Since the reflectance both in case of single-layer and gradient coatings was found to be <1% (Figures 7a and 7c), we attribute the losses in the transmittance in the coated samples to the light scattering at the larger features present in the Al_2O_3 (Figure 7b,d) formed as a result of polydispersity and/or homopolymer present in the original BCP template.

Contact angle measurements demonstrated that the Al_2O_3 SIS coatings rendered the glass surface more hydrophobic (Figure 8c). The contact angle of water droplet at the surface of uncoated glass was 32 ± 2°. Deposition of single-layer Al_2O_3 SIS coating resulted in contacted angles of 42 ± 3°. Three-layer Al_2O_3 SIS coating demonstrated a contact angle of 57 ± 3°. This trend can be explained by increased porosity of the surface.

CONCLUSIONS

In conclusion, low refractive index coatings can be successfully obtained using gas-phase SIS. We have shown that the refractive indices of inorganic coatings can be efficiently tuned by the volume fraction of the SIS-binding block in the BCP and by the number of SIS cycles. The refractive index of Al_2O_3 can be lowered down to 1.1 by SIS. We have demonstrated that the thickness of the Al_2O_3 surface coating

DOI: 10.1021/acsnano.6b08361
ACS Nano 2017, 11, 2521−2530

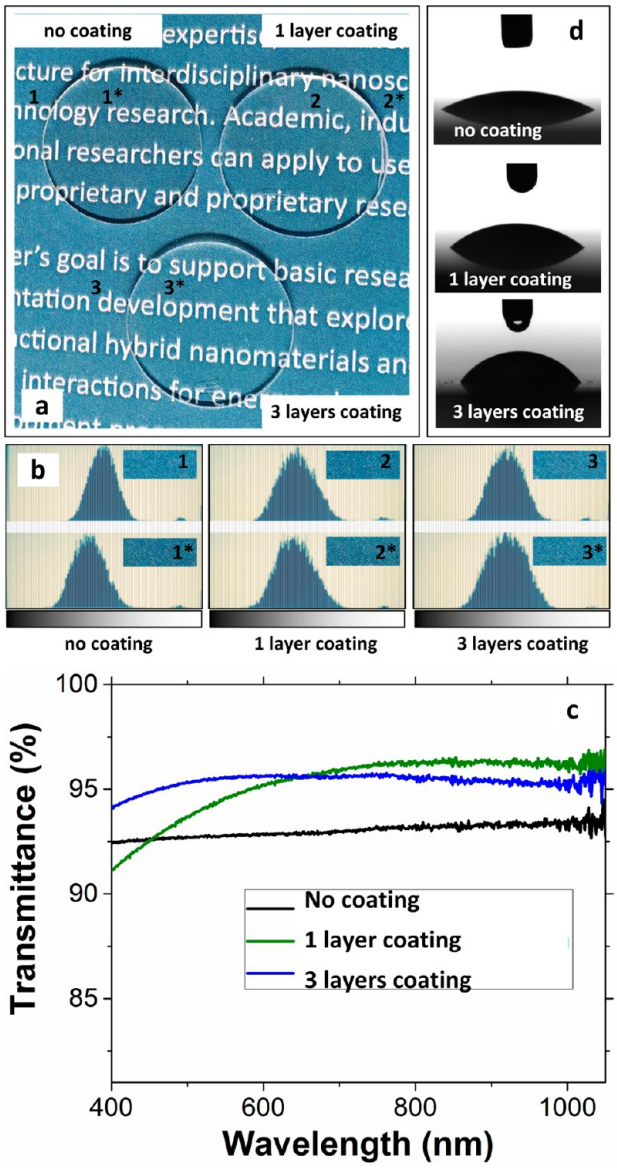

Figure 8. Photograph of uncoated glass and glass with single-layer and graded index ARCs (a). Color histograms (b) obtained for the selected areas of the blue background denoted in (a) as n and n*. (c) Transmittance spectra of glass and glass samples coated with single- and gradient three-layers aluminum oxide. (d) Photographs demonstrating the contact angle of water droplet at the surface of plain glass and glass with single-layer and graded index ARCs.

can be efficiently controlled by solvent swelling of the template, which induces porosity in the BCP and, as a result, facilitates rapid diffusion for the precursor molecules and complete infiltration of the polymer film. Control over the thickness of the SIS coating has enabled the deposition of both particular spectral range and graded-index broadband ARCs. Fresnel reflections have been shown to decrease down to 0.1% under normal illumination over a broad spectral range. The deposition of low refractive index coating by SIS is simple and robust. Since porosity and thickness of the films can be efficiently tuned in a broad range, solvent-assisted SIS does not require an artificial increase of the refractive index of the low refractivity substrate surface as is commonly accepted in the design of broad band antireflective coatings. We believe that SIS can be easily applied to a broad range of materials and can be considered as a cost-efficient alternative to the oblique-angle techniques currently used for deposition of broadband ARCs.

METHODS AND EXPERIMENTAL DETAILS

Materials. Two types of block copolymers used in the study, poly(styrene-*block*-4-vinylpyridine) (PS-*b*-P4VP) and polystyrene-*block*-poly(methyl methacrylate) (PS-*b*-PMMA) with different lengths of polar and nonpolar blocks (PS_{75k}-*b*-$PMMA_{25k}$, PS_{15k}-*b*-$PMMA_{65k}$, PS_{37k}-*b*-$PMMA_{37k}$, PS_{42k}-*b*-$PMMA_{16k}$) were purchased from Polymer Source, Inc. BCP films were prepared by spin coating from 2 and 6 wt % toluene solutions (to prepare the films of different thicknesses) onto clean silicon substrates with native silicon dioxide films and with ALD-deposited 5 nm alumina adhesion layers. Samples demonstrating antireflection properties were prepared on clean glass substrates. In the case of the glass samples, no adhesion layer was necessary for producing a uniform antireflective coatings. Cleaning of the substrates was performed as following: 20 min of sonication in acetone, followed by 20 min of sonication in isopropanol, followed by 30 min of UV ozone exposure. After BCP deposition, the samples were kept on a hot plate at 180 °C for 10 min to evaporate residual toluene and to induce microphase separation. The thicknesses of resulting polymer films varied from 70 ± 5 nm to 400 ± 12 nm for 2 and 6 wt % toluene solutions, respectively.

Sequential infiltration synthesis reactants such as trimethyl aluminum ($Al(CH_3)_3$, TMA 96%) were purchased from Sigma-Aldrich and used as received. Deionized water was used in the deposition process.

Polymer Swelling. Swelling of the polymer films to increase the film thickness and to introduce pores for rapid infiltration with metal oxide was performed by immersing the whole sample into pure ethanol, and the samples were kept at 55, 65, or 75 °C for 1 h. Upon completion, the samples were dried under nitrogen gas flow.

Sequential Infiltration Synthesis. SIS was performed using GEMStar Thermal ALD system. The Al_2O_3 coatings were produced by infiltrating the polymer films using binary reactions of TMA/H_2O. Exposure of BCP films to TMA vapor results in selective binding to polar groups in microphase separated polymer domains. Selectively bound Al-$(CH_3)_2$ reacts with water molecules in the subsequent SIS half-cycle. The SIS was performed at 90 °C (below the polymer glass transition temperatures) to avoid the flow of swelling-formed predefined polymer structures. All precursors were introduced into the reactor as room temperature vapors. Silicon or glass substrates with polymer films were loaded on a stainless steel tray and kept in a 200 sccm nitrogen flow for at least 30 min prior to deposition. One cycle of SIS was performed as follows: 10 mTorr of the synthesis reactant precursor was admitted into the reactor for 400 s. After that, the excess of the reactant was evacuated and followed by admitting 10 mTorr of H_2O for 120 s; the chamber was then purged with 200 sccm of nitrogen to remove not-infiltrated byproducts. The cycle was repeated several times to grow films of different porosity.

Thermal Annealing of the Polymers. Following SIS, the polymer component of the resulting film was removed by baking the samples in a Thermo Fisher Scientific tube furnace at 450 °C for 1 h while flowing oxygen gas at 50 sccm. Upon cooling, near-complete removal of carbon was confirmed with energy dispersive X-ray spectroscopy analysis of the film.

Characterization. Scanning electron microscopy (SEM) images were obtained using a FEI Nova 600 Nanolab dual-beam microscope with EDX capabilities. Spectroscopic ellipsometry (Horiba Uvisel Ellipsometer) was used to evaluate the film thickness and porosity. Specular reflectivity of the samples prepared on a glass substrate was measured with a Filmetrics f40 thin-film analyzer. SAXS and GISAXS data were collected at beamline 12-ID-B at Advanced Photon Source (APS). The transmittance of the samples was characterized using UV–vis spectrophotometer Cary-50. A 14 keV X-ray beam was exposed to thin-film samples using both transmission and grazing incidence reflection modes for SAXS and GISAXS measurements, respectively. The scattering data are collected with a Pilatus 2 M detector located

DOI: 10.1021/acsnano.6b08361
ACS Nano 2017, 11, 2521–2530

about 2 m away from samples. The contact angle measurements were conducted using a Krüss DSA100 drop shape analyzer.

ASSOCIATED CONTENT

Supporting Information

The Supporting Information is available free of charge on the ACS Publications website at DOI: 10.1021/acsnano.6b08361.

SEM image demonstrating the rupture of aluminum oxide films during oxygen plasma-assisted polymer removal. EDS analysis on Al_2O_3 film obtained by thermally annealing of SIS sample (PDF)

AUTHOR INFORMATION

Corresponding Authors

*E-mail: Diana.Berman@unt.edu.
*E-mail: eshevchenko@anl.gov.

ORCID

Byeongdu Lee: 0000-0003-2514-8805
Elena V. Shevchenko: 0000-0002-5565-2060

Notes

The authors declare no competing financial interest.

ACKNOWLEDGMENTS

Work at the Center for Nanoscale Materials and Advanced Photon Source was supported by a U.S. Department of Energy Office of Science User Facility under Contract No. DE-AC02-06CH11357. The authors thank Dr. Leonidas Ocola for fruitful discussions and help with the ALD/SIS instrument. The authors acknowledge Dr. Gary Wiederrecht, Dr. Richard Schaller, Dr. Xuedan Ma, Dr. David Gosztola, and Dr. John Harvey for helpful discussions on optical properties of antireflective coatings.

REFERENCES

(1) Guldin, S.; Kohn, P.; Stefik, M.; Song, J.; Divitini, G.; Ecarla, F.; Ducati, C.; Wiesner, U.; Steiner, U. Self-Cleaning Antireflective Optical Coatings. *Nano Lett.* **2013**, *13*, 5329−5335.

(2) Buskens, P.; Burghoorn, M.; Mourad, M. C. D.; Vroon, Z. Antireflective Coatings for Glass and Transparent Polymers. *Langmuir* **2016**, *32*, 6781−6793.

(3) Raut, H. K.; Ganesh, V. A.; Nair, A. S.; Ramakrishna, S. Anti-reflective Coatings: A Critical, In-Depth Review. *Energy Environ. Sci.* **2011**, *4*, 3779−3804.

(4) Woodhead Publishing Series in Electronic and Optical Materials. In *Optical Thin Films and Coatings*; Piegary, A., Flory, F., Eds. Woodhead Publishing: Cambridge, U.K., 2013.

(5) Xi, J. Q.; Kim, J. K.; Schubert, E. F. Silica Nanorod-Array Films with Very Low Refractive Indices. *Nano Lett.* **2005**, *5*, 1385−1387.

(6) Dodge, M. J. Refractive Properties of Magnesium Fluoride. *Appl. Opt.* **1984**, *23*, 1980−1985.

(7) Xi, J. Q.; Schubert, M. F.; Kim, J. K.; Schubert, E. F.; Chen, M. F.; Lin, S. Y.; Liu, W.; Smart, J. A. Optical Thin-Film Materials with Low Refractive Index for Broadband Elimination of Fresnel Reflection. *Nat. Photonics* **2007**, *1*, 176−179.

(8) Zou, L. P.; Li, X. G.; Zhang, Q. H.; Shen, J. An Abrasion-Resistant and Broadband Antireflective Silica Coating by Block Copolymer Assisted Sol-Gel Method. *Langmuir* **2014**, *30*, 10481−10486.

(9) Hiller, J.; Mendelsohn, J. D.; Rubner, M. F. Reversibly Erasable Nanoporous Anti-Reflection Coatings from Polyelectrolyte Multilayers. *Nat. Mater.* **2002**, *1*, 59−63.

(10) Li, Y.; Liu, F.; Sun, J. Q. A Facile Layer-by-Layer Deposition Process for the Fabrication of Highly Transparent Superhydrophobic Coatings. *Chem. Commun.* **2009**, 2730−2732.

(11) Burghoorn, M.; Roosen-Melsen, D.; de Riet, J.; Sabik, S.; Vroon, Z.; Yakimets, I.; Buskens, P. Single Layer Broadband Anti-Reflective Coatings for Plastic Substrates Produced by Full Wafer and Roll-to-Roll Step-and-Flash Nano-Imprint Lithography. *Materials* **2013**, *6*, 3710−3726.

(12) Leem, J. W.; Yu, J. S. Wafer-Scale Highly-Transparent and Superhydrophlic Sapphires for High Performance Optics. *Opt. Express* **2012**, *20*, 26160−26166.

(13) Ye, X.; Huang, J.; Geng, F.; Liu, H.; Sun, L.; Yan, L.; Jiang, X.; Wu, W.; Zheng, W. High Power Laser Antireflection Subwavelength Grating on Fused Silica by Colloidal Lithography. *J. Phys. D: Appl. Phys.* **2016**, *49*, 265104.

(14) Ye, X.; Jiang, X.; Huang, J.; Geng, F.; Sun, L.; Zu, X.; Wu, W.; Zheng, W. Formation of Broadband Antireflective and Superhydrophilic Subwavelength Structures on Fused Silica Using OneStep Self-Masking Reactive Ion Etching. *Sci. Rep.* **2015**, *5*, 13023.

(15) Stefik, M.; Guldin, S.; Vignolini, S.; Wiesner, U.; Steiner, U. Block Copolymer Salf-Assembly for Nanophotonics. *Chem. Soc. Rev.* **2015**, *44*, 5076−5091.

(16) Blumstein, A. Polymerization of Adsorbed Monolayers. II. Thermal Degradation of the Inserted Polymer. *J. Polym. Sci., Part A: Gen. Pap.* **1965**, *3*, 2665−2672.

(17) Prevo, B. G.; Hwang, Y.; Velev, O. D. Convective Assembly of Antireflective Silica Coatings with Controlled Thickness and Refractive Index. *Chem. Mater.* **2005**, *17*, 3642−3651.

(18) Kennedy, S. R.; Brett, M. J. Porous Broadband Antireflection Coating by Glancing Angle Deposition. *Appl. Opt.* **2003**, *42*, 4573−4579.

(19) Biswas, M.; Libera, J. A.; Darling, S. B.; Elam, J. W. New Insight into the Mechanism of Sequential Infiltration Synthesis from Infrared Spectroscopy. *Chem. Mater.* **2014**, *26*, 6135−6141.

(20) Peng, Q.; Tseng, Y. C.; Darling, S. B.; Elam, J. W. Nanoscopic Patterned Materials with Tunable Dimensions *via* Atomic Layer Deposition on Block Copolymers. *Adv. Mater.* **2010**, *22*, 5129−5133.

(21) Peng, Q.; Tseng, Y. C.; Darling, S. B.; Elam, J. W. A Route to Nanoscopic Materials *via* Sequential Infiltration Synthesis on Block Copolymer Templates. *ACS Nano* **2011**, *5*, 4600−4606.

(22) Tseng, Y.-C.; Peng, Q.; Ocola, L. E.; Czaplewski, D. A.; Elam, J. W.; Darling, S. B. Etch Properties of Resists Modified by Sequential Infiltration Synthesis. *J. Vac. Sci. Technol., B: Nanotechnol. Microelectron.: Mater., Process., Meas., Phenom.* **2011**, *29*, 06FG01.

(23) Tseng, Y.-C.; Peng, Q.; Ocola, L. E.; Elam, J. W.; Darling, S. B. Enhanced Block Copolymer Lithography Using Sequential Infiltration Synthesis. *J. Phys. Chem. C* **2011**, *115*, 17725−17729.

(24) Black, C. T.; Ruiz, R.; Breyta, G.; Cheng, J. Y.; Colburn, M. E.; Guarini, K. W.; Kim, H. C.; Zhang, Y. Polymer Self Sssembly in Semiconductor Microelectronics. *IBM J. Res. Dev.* **2007**, *51*, 605−633.

(25) Checco, A.; Rahman, A.; Black, C. T. Robust Superhydrophobicity in Large-Area Nanostructured Surfaces Defined by Block-Copolymer Self Assembly. *Adv. Mater.* **2014**, *26*, 886−891.

(26) Ruiz, R.; Kang, H.; Detcheverry, F. A.; Dobisz, E.; Kercher, D. S.; Albrecht, T. R.; de Pablo, J. J.; Nealey, P. F. Density Multiplication and Improved Lithography by Directed Block Copolymer Assembly. *Science* **2008**, *321*, 936−939.

(27) Biswas, M.; Libera, J. A.; Darling, S. B.; Elam, J. W. Kinetics for the Sequential Infiltration Synthesis of Alumina in Poly(methyl methacrylate): An Infrared Spectroscopic Study. *J. Phys. Chem. C* **2015**, *119*, 14585−14592.

(28) Kim, H. C.; Park, S. M.; Hinsberg, W. D. Block Copolymer Based Nanostructures: Materials, Processes, and Applications to Electronics. *Chem. Rev.* **2010**, *110*, 146−177.

(29) Bang, J.; Jeong, U.; Ryu, D. Y.; Russell, T. P.; Hawker, C. J. Block Copolymer Nanolithography: Translation of Molecular Level Control to Nanoscale Patterns. *Adv. Mater.* **2009**, *21*, 4769−4792.

(30) Groner, M. D.; Fabreguette, F. H.; Elam, J. W.; George, S. M. Low-Temperature Al2O3 Atomic Layer Deposition. *Chem. Mater.* **2004**, *16*, 639−645.

DOI: 10.1021/acsnano.6b08361
ACS Nano 2017, 11, 2521−2530

(31) Wang, Y. Nondestructive Creation of Ordered Nanopores by Selective Swelling of Block Copolymers: Toward Homoporous Membranes. *Acc. Chem. Res.* **2016**, *49*, 1401−1408.
(32) Yin, J.; Yao, X.; Liou, J.-Y.; Sun, W.; Sun, Y.-S.; Wang, Y. Membranes with Highly Ordered Straight Nanopores by Selective Swelling of Fast Perpendicularly Aligned Block Copolymers. *ACS Nano* **2013**, *7*, 9961−9974.
(33) Lee, B.; Yoon, J.; Oh, W.; Hwang, Y.; Heo, K.; Jin, K. S.; Kim, J.; Kim, K. W.; Ree, M. In-situ Grazing Incidence Small-Angle X-ray Scattering Studies on Nanopore Evolution in Low-k Organosilicate Dielectric Thin Films. *Macromolecules* **2005**, *38*, 3395−3405.
(34) Lee, B. D.; Park, Y. H.; Hwang, Y. T.; Oh, W.; Yoon, J.; Ree, M. Ultralow-k Nanoporous Organosilicate Dielectric Films Imprinted with Dendritic Spheres. *Nat. Mater.* **2005**, *4*, 147−151.
(35) Elam, J. W.; Routkevitch, D.; Mardilovich, P. P.; George, S. M. Conformal Coating on Ultrahigh-Aspect-Ratio Nanopores of Anodic Alumina by Atomic Layer Deposition. *Chem. Mater.* **2003**, *15*, 3507−3517.
(36) Rywak, A. A.; Burlitch, J. M. Sol−Gel Synthesis of Nanocrystalline Magnesium Fluoride: Its Use in the Preparation of MgF2 Films and MgF2−SiO2 Composites. *Chem. Mater.* **1996**, *8*, 60−67.
(37) Dobrowolski, J. A.; Guo, Y. N.; Tiwald, T.; Ma, P. H.; Poitras, D. Toward Perfect Antireflection Coatings. 3. Experimental Results Obtained with the Use of Reststrahlen Materials. *Appl. Opt.* **2006**, *45*, 1555−1562.
(38) Dobrowolski, J. A.; Poitras, D.; Ma, P.; Vakil, H.; Acree, M. Toward Perfect Antireflection Coatings: Numerical Investigation. *Appl. Opt.* **2002**, *41*, 3075−3083.
(39) Poitras, D.; Dobrowolski, J. A. Toward Perfect aAntireflection Coatings. 2. Theory. *Appl. Opt.* **2004**, *43*, 1286−1295.

DOI: 10.1021/acsnano.6b08361
ACS Nano 2017, 11, 2521−2530